New Zn(II) complexes based on biologically active substituted acetic acid and nitrogen donor ligands: synthesis, crystal structure and biological applications

Shayma Kamel, Hijazi Abu Ali & Amani Abu Shamma

Taylor & Francis
Taylor & Francis Group

Check for updates

New Zn(II) complexes based on biologically active substituted acetic acid and nitrogen donor ligands: synthesis, crystal structure and biological applications

Shayma Kamel[1], Hijazi Abu Ali[1] (ID) and Amani Abu Shamma

Department of Chemistry, Birzeit University, West Bank, Palestine

ABSTRACT

The complexes [Zn(phenylacetato)$_2$(2-aminopyridin)$_2$] (**3**), [Zn(phenylacetato)$_2$(1,10-phenanthroline)]·H$_2$O (**4**), and [Zn(phenylacetato)$_2$(2,9-dimethyl-1,10-phenanthroline)]·0.5 H$_2$O (**5**) were prepared and characterized by IR-, UV–Visible, ^{1}H and ^{13}C NMR spectroscopy, and single crystal X-ray diffraction. BNPP hydrolysis of the complexes and their parent nitrogen ligands showed that the hydrolysis rate of *bis*-(4-nitrophenyl) phosphate (BNPP) was 1.7×10^5 L mol^{-1} s^{-1} for **3**, 3.1×10^5 L mol^{-1} s^{-1} for **4** and 4.3×10^4 L mol^{-1} s^{-1} for **5**. Antibacterial activities show the effect of complexation on activity against Gram-positive (*S. epidermidis*, *S. aureus*, *E. faecalis*, *M. luteus* and *B. subtilis*) and Gram-negative (*K. pneumonia*, *E. coli*, *P. mirabilis* and *P. aeruginosa*) bacteria using the agar well diffusion method. Complex **4** showed good activity against G− bacteria except *P. aeruginosa*, and against G+ bacteria except *E. ferabis*. Complex **5** showed no activity against G− bacteria, low activity against *M. luteus* and *B. subtilis* bacteria and high activity against *S. epidemidis* and *S. aureus*. Complex **3** did not show any activity against G− or G+ bacteria.
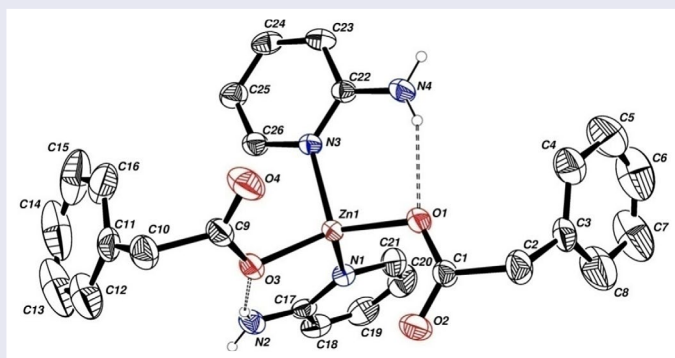
CONTACT Hijazi Abu Ali ✉ habuali@birzeit.edu, habuali1@yahoo.com
[1] These authors contributed equally to this work.

1. Introduction

The metabolism and transport of metal ions and their complexes have been studied [1]. All biological activities of metals are due to their characteristics such as redox activity, many coordination modes, and reactivity toward organic substrates [2]. There are four major categories for the essential chemical elements: (a) bulk elements (H, C, N, O, P, S), (b) macrominerals and ions (Na, K, Mg, Ca, Cl, PO_4^{-3}, SO_4^{-2}), (c) trace elements (Fe, Zn, Cu), and (d) ultratrace elements that involve nonmetals (F, I, Se, Si, As, B) and metals (Mn, Mo, Co, Cr, V, Ni, Cd, Sn, Pb, Li); each essential element has approximate percentages by weight for an adult human [3]. Zinc is relatively abundant and is essential for many biological processes and must be included in the diet for optimum health [4].

Carboxylic acids can be ligands and have many biological activities such as anti-inflammatory effect (ibuprofen, naproxen, and tolmetin) [5]. The antibacterial activities of nalidixic acid can be enhanced by complexation with metal ions. However, in other similar complexes the activities were decreased [6].

Recently, studies on the antimicrobial activity of Nonsteroidal Anti-Inflammatory Drugs (NSAIDs) showed increased activity when complexed with transition metals and various nitrogen ligands [7]. Several metal complexes accelerate the drug action and efficacy of organic therapeutic agents, e.g. Co(II) complexes bearing mefenamic acid [8], naproxen [9] or tolfenamic acid [10], and Mn(II) complexes of tolfenamic acid [11] have been studied as anti-inflammatory agents. In addition, Cu(II) complexes of mefenamic acid, naproxen, diclofenac [12] diflunisal [13], and flufenamic acid [14] have been reported. Zinc complexes with biologically active ligands have pharmaceutical effects because they can catalyze enzymatic processes in biological systems, e.g. zinc(II) aliphatic carboxylates with nitrogen-based ligands (like valproic acid) [15, 16] and aromatic carboxylates with nitrogen-based ligands (like naproxen, ibuprofen, Indomethacin…) have been synthesized and studied as antibacterial and antimalarial agents [17–20].

Phosphate hydrolysis has an important role in many biological and environmental applications. For example, this hydrolysis represents the cleavage of the phosphorus bond as shown in scheme 1.

A hydroxamic acid (HL) containing benzo-15-crown-5 and their copper(II), zinc(II), cobalt(II), and manganese(II) complexes have been synthesized and studied as catalysts [21, 22]. The catalytic properties of these complexes and the kinetics and mechanism of BNPP hydrolysis were investigated. Moreover, the kinetic mathematical model of BNPP cleavage catalyzed by these complexes has been proposed [21, 22].

Rapid hydrolysis of the high stable phosphate diester bond in *bis*-(4-nitrophenyl) phosphate (BNPP) by enzymes or catalysts containing metal ion complexes have recently been achieved [21, 22].

2. Experimental

2.1. Chemicals, materials and biological species

All reagents, chemicals and solvents were purchased from commercial sources and were used without purification.
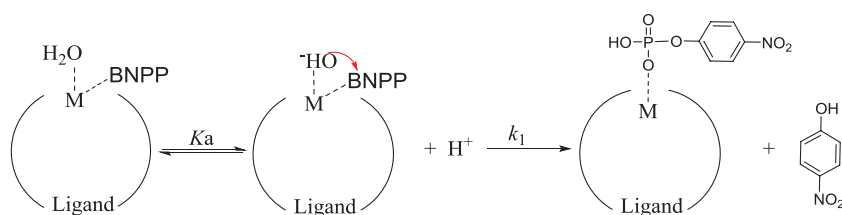
Scheme 1. Phosphate hydrolysis of BNPP.

2.2. Physical measurements

Solid samples with anhydrous potassium bromide (KBr) were ground and compressed into a disc to use for IR spectral measurements, which were recorded from 200 to 4000 cm^{-1} on a TENSOR II (BRUKER) FT–IR Spectrometer. UV–Vis spectra were recorded on an Agilent 8453 photodiode array (PDA) spectrophotometer from 200 to 600 nm using CH_3OH as solvent. NMR spectra were recorded on a Varian Unity Spectrometer operating at 300 MHz for ^{1}H and ^{13}C nuclei. Melting points were determined in capillary tubes with an Electrothermal apparatus and Bruker SMART APEX CCD X-ray diffractometer was used for X-ray data.

2.3. Synthesis and characterization of zinc(II) compounds

All zinc(II) compounds were prepared at room temperature.

2.3.1. [bis-(phenylacetato)zinc(II)] (2)

Sodium hydroxide (1.0 mmol, 1.5 g) and phenyl acetic acid (1.0 mmol, 5.0 g) in 100 mL of MeOH were stirred for 3 h. Then the solvent was evaporated to give a needle solid which was redissolved in MeOH and $ZnCl_2$ (1.0 mmol, 5.0 g) in 15 mL of MeOH was added to it with stirring. The reaction mixture was stirred for an additional 12 h; the obtained white precipitate was then filtered, washed with cold water and air dried to give 4.4 g of solid product.

[**Zn($C_8H_7O_2$)$_2$**] (**2**). 89% yield; m.p. > 200 °C; ^{1}H NMR (CDCl$_3$): δ (ppm) 3.39 (s, 2H, CH$_2$), 7.21 (s, 5H, CH); ^{13}C{^{1}H}-NMR (CDCl$_3$): δ (ppm) 43.11 (CH$_2$), 126.21 (CH), 128.31 (CH), 129.69 (CH), 137.91 (C), 176.98 (C=O); IR (cm^{-1}, KBr): 3444, 2350, 1531, 1439, 1391, 723; UV–Vis (MeOH, λ(nm)): 214, 259, 265.

2.3.2. [Zn(phenylacetato)$_2$(2-aminopyridine)$_2$] (3)

2-Aminopyridine (4 mmol, 0.38 g) dissolved in a minimum of MeOH was added with stirring to a 50 mL MeOH solution of [*bis*-(phenylacetato)zinc(II)] (2.0 mmol, 0.40 g), then the clear reaction mixture was stirred for an additional 7 h. The solution was allowed to evaporate to give solid crystals. Crystals for X-ray structural analysis were obtained by recrystallization from CH$_2$Cl$_2$.

[**Zn($C_8H_7O_2$)$_2$($C_5H_6N_2$)$_2$**] (**3**). 77% yield; m.p. = 147–149 °C; ^{1}H NMR (CDCl$_3$): δ (ppm) 3.64 (s, 2H, CH$_2$), 5.78 (s, 2H, NH$_2$), 6.39 (d, 1H, CH, $^3J_{H-H}$ = 8.4 Hz), 6.47 (t, 1H, CH, $^3J_{H-H}$ = 12.9 Hz), 7.20 (m, 1H, CH), 7.26 (m, 5H, CH), 7.37 (m, 1H, CH), 7.74 (d, 1H, CH, $^3J_{H-H}$ = 5.4 Hz); ^{13}C{^{1}H}-NMR (CDCl$_3$): δ (ppm) 43.60 (CH$_2$), 111.43 (CH), 112.96 (CH), 122.96 (CH), 126.10 (CH), 128.18 (CH), 129.52 (CH), 137.16 (C), 139.73 (CH), 145.97 (CH), 159.05 C(NH$_2$), 178.52 (C=O); IR (cm^{-1},

KBr): 3341, 3227, 3024, 2700, 1619, 1567, 1499, 1360, 1271, 1159, 851, 698, 661; UV–Vis (MeOH, λ (nm)): 296.

2.3.3. [Zn(phenylacetato)$_2$(1,10-phenanthroline)]monohydrate (4)

1,10-Phenanthroline (2.0 mmol, 0.36 g) dissolved in minimum amount of MeOH was added with stirring to [bis-(phenylacetato)zinc(II)] (2.0 mmol, 0.40 g) dissolved in 50 mL MeOH. The clear solution of the reaction mixture was stirred for an additional 7 h, then was allowed to evaporate and solid crystals were obtained. Suitable crystals for X-ray structural analysis were obtained by recrystallization from MeOH.

[Zn(C$_8$H$_7$O$_2$)$_2$(C$_{13}$H$_{12}$N$_2$)]·H$_2$O (4). 85% yield; m.p. = 101 °C; ^{1}H NMR (CDCl$_3$): δ (ppm) 3.63 (s, 2H, CH$_2$), 7.19 (m, 5H, CH), 7.68 (t, 2H, CH, $^3J_{H-H}$ = 12.6 Hz), 7.76 (s, 2H, CH), 8.32 (d, 2H, CH, $^3J_{H-H}$ = 8.1 Hz), 9.05 (d, 2H, CH, $^3J_{H-H}$ = 4.8 Hz); ^{13}C{^{1}H}-NMR (CDCl$_3$): δ (ppm) 43.43 (CH$_2$), 124.28 (CH), 125.03 (CH), 126.04(CH), 126.58 (CH), 128.11(CH), 128.45 (C), 129.39 (CH), 137.06 (C), 138.85 (CH), 150.12 (CH), 180.59 (C=O); IR (cm^{-1}, KBr): 1998, 1515, 1223, 1144, 1100, 853; UV–Vis (MeOH, λ (nm)): 277, 292, 325.

2.3.4. [Zn(phenylacetato)$_2$(2,9-dimethyl-1,10-phen)] hemihydrate (5)

2,9-Dimethyl-1,10-phen (2.0 mmol, 0.45 g) dissolved in a minimum of MeOH was added with stirring to [bis-(phenylacetato)zinc(II)] (2.0 mmol, 0.40 g) dissolved in 50 mL MeOH. The clear solution of the reaction mixture was stirred for an additional 7 h, then was allowed to evaporate and solid crystals were obtained. Suitable crystals for X-ray structural analysis were obtained by recrystallization from MeOH.

[Zn(C$_8$H$_7$O$_2$)$_2$(C$_{15}$H$_{16}$N$_2$)]·0.5H$_2$O (5). 79% yield; m.p. = 159–165 °C; ^{1}H NMR (CDCl$_3$): δ (ppm) 2.99 (s, 3H, CH$_3$), 3.66 (s, 2H, CH$_2$), 7.15 (t, 2H, CH, $^3J_{H-H}$ = 15.6 Hz), 7.21 (d, 2H, CH, $^3J_{H-H}$ = 6.9 Hz), 7.28 (d, 2H, CH, $^3J_{H-H}$ = 7.2 Hz), 7.54 (d, 2H, CH, $^3J_{H-H}$ = 8.4 Hz), 7.64 (s, 2H, CH), 8.19 (d, 2H, CH, $^3J_{H-H}$ = 8.4 Hz); ^{13}C{^{1}H}-NMR (CDCl$_3$): δ (ppm) 24.78 (CH$_3$), 43.05 (CH$_2$), 125.55 (CH), 125.99 (CH), 126.25 (C), 126.86 (CH), 128.10 (CH), 129.35 (CH), 137.35 (C), 139.09 (CH), 140.1 9 (C), 160.73 (C), 179.04 (C=O); IR (cm^{-1}, KBr): 3027, 2800, 1500, 1450, 1340, 1221, 861; UV–Vis (MeOH, λ (nm)): 201, 231 269.

2.4. X-ray crystallography

Single crystal X-ray analyses of **3**, **4**, and **5** were carried out by attaching single crystals to a glass fiber with epoxy glue, and then transferring to the X-ray diffractometer system (Bruker SMART APEX CCD) which is controlled by using a Pentium-based PC running the SMART software package [23]. The diffracted graphite monochromated (Kα radiation λ = 0.71073 Å) was detected on a phosphor screen at −44 °C, held at 6.0 cm from the crystal. A detector array of 512 × 512 pixels (a pixel size ≈ 120 μm) was used to collect data [24]. Crystal data and structure refinements are summarized in tables 1 and 2.

2.5. Kinetic measurements of BNPP hydrolysis

Optimum concentrations and conditions for the BNPP hydrolysis were chosen by running different UV–Visible kinetic experiments and the best absorbance versus time plots were used to determine the optimum conditions.

Table 1. Structure refinement and crystal data for **3** and **4**.

	3	4
Empirical formula	$C_{26}H_{26}N_4O_4Zn$	$C_{28}H_{22}N_2O_5Zn$
Formula weight	523.88	531.85
Temperature	293(1) K	293(1) K
Wavelength	0.71073 Å	0.71073 Å
Crystal system	Triclinic	Monoclinic
Space group	P-1	P2(1)/c
Unit cell dimensions	$a = 10.877(2)$ Å, $\alpha = 87.918(4)°$	$a = 10.589(1)$ Å, $\alpha = 90°$
	$b = 11.204(2)$ Å, $\beta = 74.302(4)°$	$b = 11.165(2)$ Å, $\beta = 97.681(2)°$
	$c = 11.461(3)$ Å, $\gamma = 75.807(4)°$	$c = 12.160(3)$ Å, $\gamma = 90°$
Volume	1302.9(5) Å³	2438.3(6) Å³
Z	2	4
Density (calculated)	1.335 Mg m⁻³	1.449 Mg m⁻³
Absorption coefficient	0.980 mm⁻¹	1.049 mm⁻¹
F(0 0 0)	544	1096
Crystal size	$0.36 \times 0.36 \times 0.13$ mm³	$0.36 \times 0.29 \times 0.26$ mm³
Theta range for data collection	2.39 to 28.01°	2.20 to 27.00°
Index ranges	$-14 \leq h \leq 14, -14 \leq k \leq 14, -15 \leq l \leq 14$	$-13 \leq h \leq 13, -23 \leq k \leq 23, -16 \leq l \leq 16$
Reflections collected	15,064	26,565
Independent reflections	6067 [R(int) = 0.0258]	5314 [R(int) = 0.0306]
Completeness to θ = 28.03°	96.4%	99.8%
Absorption correction	Multi-scan	Semi-empirical from equivalents
Max. and min. transmission	0.8832 and 0.7193	0.7720 and 0.7038
Data/restraints/parameters	6067/4/332	5314/0/325
Goodness-of-fit on F^2	1.122	1.197
[a]Final R indices [$I > 2\sigma (I)$]	$R_1 = 0.0591, wR_2 = 0.1440$	$R_1 = 0.0519, wR_2 = 0.1213$
R indices (all data)	$R_1 = 0.0722, wR_2 = 0.1514$	$R_1 = 0.0576, wR_2 = 0.1244$
Largest diff. peak and hole	0.526 and −0.397 e.Å⁻³	0.533 and −0.439 e.Å⁻³

[a]$R_1 = \Sigma||Fo| - |Fc||/\Sigma|Fo|$ and $wR_2 = \{\Sigma[w(F0^2 - Fc^2)^2]/\Sigma[w(Fo^2)^2]\}^{1/2}$

Table 2. Structure refinement and crystal data for **5**.

Empirical formula	$C_{30}H_{27}N_2O_{4.50}Zn$
Formula weight	552.91
Temperature	296(1) K
Wavelength	0.71073 Å
Crystal system	Monoclinic
Space group	C2/c
Unit cell dimensions	$a = 29.017(6)$ Å, $\alpha = 90°$
	$b = 12.615(2)$ Å, $\beta = 100.401(2)°$
	$c = 14.667(3)$ Å, $\gamma = 90°$
Volume	5280(2) Å³
Z	8
Density (Calcd)	1.391 Mg m⁻³
Absorption coefficient	0.971 mm⁻¹
F(0 0 0)	2296
Crystal size	$0.42 \times 0.16 \times 0.10$ mm³
Theta range for data collection	2.68 to 27.00°
Index ranges	$-36 \leq h \leq 36, -14 \leq k \leq 16, -18 \leq l \leq 18$
Reflections collected	19,220
Independent reflections	5684 [R(int) = 0.0581]
Completeness to θ = 28.03°	98.4%
Absorption correction	Semi-empirical from equivalents
Max. and min. transmission	0.9092 and 0.6859
Data/restraints/parameters	5684/0/341
Goodness-of-fit on F^2	0.851
[a]Final R indices [$I > 2\sigma (I)$]	$R_1 = 0.0546, wR_2 = 0.1425$
R indices (all data)	$R_1 = 0.1619, wR_2 = 0.1740$
Largest diff. peak and hole	0.270 and −0.324 e.Å⁻³

[a]$R_1 = \Sigma||Fo| - |Fc||/\Sigma|Fo|$ and $wR_2 = \{\Sigma[w(F0^2 - Fc^2)^2]/\Sigma[w(Fo^2)^2]\}^{1/2}$

The following conditions were used for all hydrolysis reactions: HEPES"4-(2-hydroxyethyl)-1-piperazineethanesulfonic acid" buffer with concentration of 50 µM was prepared by dissolving the appropriate amount in a minimum amount of deionized water, then controlling the pH to 7.91 using HCl or NaOH and the final volume was adjusted to 100 mL. BNPP (0.036 g) was dissolved in the prepared buffer to obtain a concentration of 1 mM. The desired complex concentration was prepared using methanol as a solvent; the two solutions were kept in a water bath at 25 °C for 10 min, then (1.5 mL) of the two solutions were mixed in a quartz cell at 25 °C, the rate of release of p-nitrophenol was directly measured using UV–Vis spectrophotometer at $\lambda = 400$ nm and an extinction coefficient of 13,400 Lmol^{-1} cm^{-1}. The concentration effect of BNPP solution on the hydrolysis process was measured by preparing 10^{-4} and 10^{-5} M solutions and the rate of hydrolysis was calculated [25].

3. Results and discussion

3.1. Synthesis of Zn(II) complexes

The proposed structure of [*bis*-(phenylacetato)zinc(II)] **2** and **3**, **4** and **5** are shown in schemes 2 and 3, respectively.

Nitrogen donor ligands were mixed with **2** in various ratios as shown in the Experimental section. The proposed structures are supported by their single crystal X-ray structure determination. The physical properties and yield of the prepared zinc(II) complexes are listed in table 3.
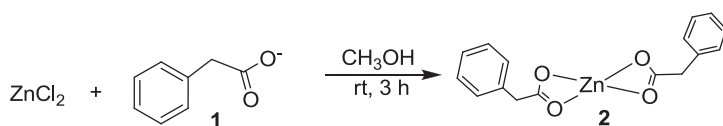
Scheme 2. Synthesis and proposed structure of zinc(II) complexes.
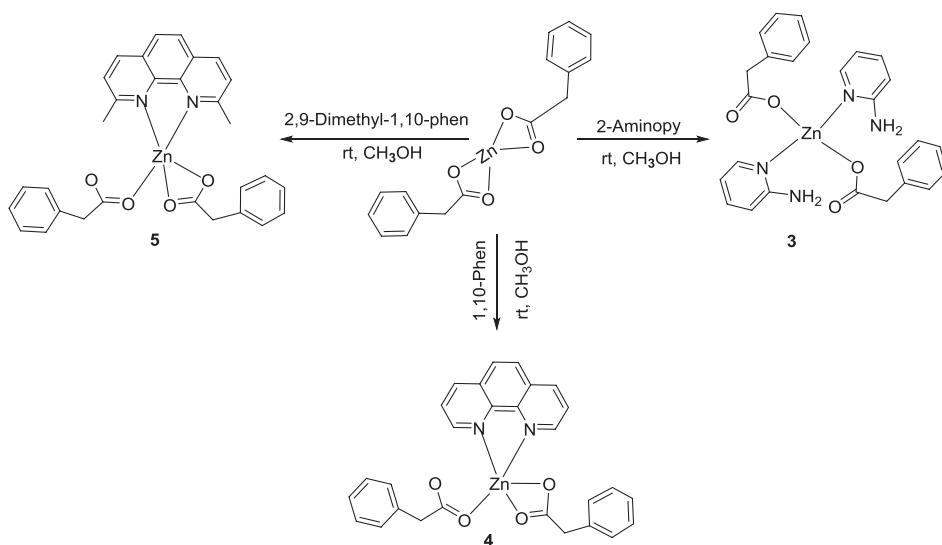
Scheme 3. Synthesis and proposed structure of the zinc(II) complexes.

3.2. Crystallographic study

3.2.1. X-ray crystal structure of 3

As shown in figure 1, Zn(II) is bound to two monodentate phenyl acetate and two monodentate 2-ampy ligands. The Zn(1)–O(1) bond of 1.942(2) Å and Zn(1)–O(3) 1.9359(19) Å and Zn(1)–N(1) 2.056(3) Å and Zn(1)–N(3) 2.048(2) Å bond distances are obtained. Selected bond distances and angles are listed in table S1 (Supporting Material).

Complex **3** adopted slightly distorted tetrahedral geometry around Zn(II), O(1)-Zn(1)-O(3) = 129.09(10)°, N(1)–Zn(1)–N(3) = 99.19(10)°, N(1)–Zn(1)–O(1) = 108.34(10)°, N(3)–Zn(1)–O(3) = 106.05(9)°.

Further stability of the crystal lattice was gained by intramolecular hydrogen bonding. Table 4 shows the H-bond distances in (Å), where these bonds are between O(1), O(2), O(3) and O(4) of the phenyl acetate groups and H of the amino groups as represented by the dashed lines within a single molecule.

3.2.2. X-ray crystal structure of 4

The atomic scheme and atom connectivity for **4** are shown in figure 2, in which Zn(II) is covalently bonded to one monodentate phenyl acetate group, one bidentate phenyl acetate and one bidentate 1,10-phen. Selected interatomic distances and angles are found in table S2.

Table 3. Physical properties and yield of zinc(II) complexes.

Compounds	%Yield	m.p (°C)	Solubility
3	77	147–149	$CHCl_3$, CH_3OH, $CH_3C(O)CH_3$, DMSO
4	85	101	$CHCl_3$, CH_3OH
5	79	159–165	CH_3OH, $CH_3C(O)CH_3$, DMSO

Figure 1. View of the molecular structure of **3** showing the atom numbering scheme. Ellipsoids represent thermal displacement parameters at the 25% probability level and hydrogens in calculated positions have been omitted for clarity.

Table 4. Hydrogen bonds for **3** [Å and °].

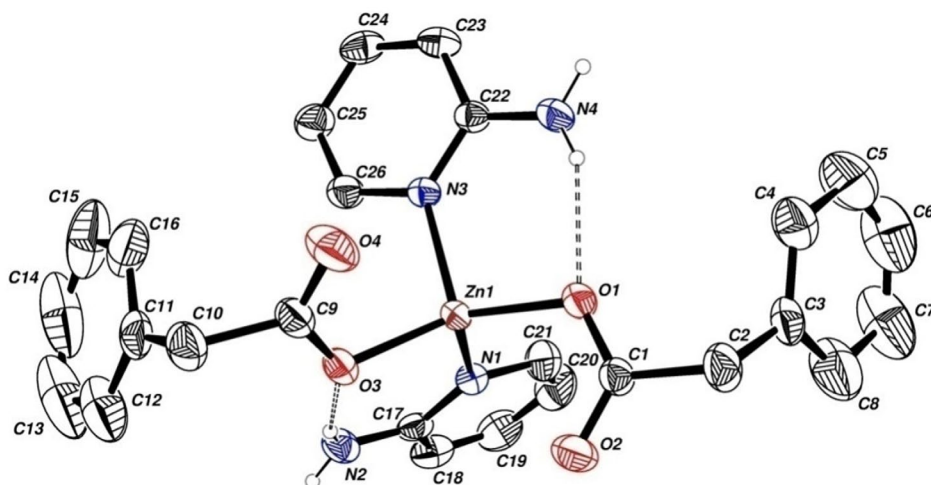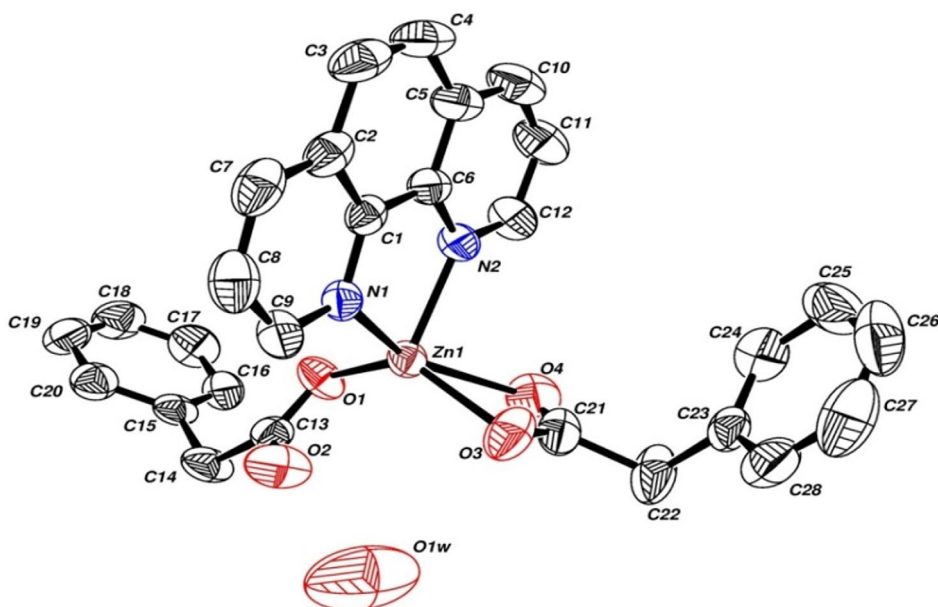| D–H⋯A	d(D–H)	d(H⋯A)	d(D⋯A)	<(DHA)
N(2)–H(1N2)⋯O(2)#1	0.819(10)	2.112(11)	2.931(4)	179(3)
N(2)–H(2N2)⋯O(3)	0.815(10)	2.090(15)	2.873(4)	161(3)
N(4)–H(1N4)⋯O(4)#2	0.811(10)	2.194(15)	2.971(4)	160(3)
N(4)–H(2N4)⋯O(1)	0.817(10)	2.140(17)	2.901(4)	155(3)

Figure 2. View of the molecular structure of **4** showing the atom numbering scheme. Ellipsoids represent thermal displacement parameters at the 50% probability level and hydrogens in calculated positions have been omitted for clarity.

Complex **4** adopted slightly distorted trigonal bipyramidal geometry around Zn(II) with O(3)–Zn(1)–O(4) = 58.56(10)°, N(1)–Zn(1)–N(2) = 79.40(8)°, N(1)–Zn(1)–O(3) = 104.10(8)°, O(1)–Zn(1)–N(2) = 109.19(8)°.

The water (O1w) is positioned between (O2) of the phenyl acetate groups at 2.879 Å, (O3) at a distance of 3.231 Å and to another (O1w) at a distance of 3.655 Å. The water molecule is disordered so the hydrogens could not be found.

3.2.3. X-ray crystal structure of 5

The atomic scheme and atom connectivity for **5** are shown in figure 3, in which Zn(II) is covalently bonded to one monodentate phenylacetate group, one bidentate phenylacetate and one bidentate 2,9-dmp. Selected interatomic distances and angles are found in table S3. Complex **5** has slightly distorted trigonal bipyramidal geometry around Zn(II), O(1)– Zn(1)–O(4) = 111.81(19)°,   N(1)–Zn(1)–N(2) = 80.8(3)°,   O(1)–Zn(1)–N(2) = 110.45(16)°, N(1)–Zn(1)–O(3) = 100.1(2)°.

The water (O1w) is positioned between two carbonyl groups (O2) of the phenylacetate group from two neighbor complexes at 2.674 Å. The water molecule is disordered so the hydrogens could not be found.

3.3. IR spectroscopy

Infrared spectral data of sodium phenylacetate complexes from 400 to 4000 cm^{-1} as KBr pellets are summarized in table 5.

In metal carboxylate complexes, the major characteristic of the IR spectra is the frequency of the v asymmetric (v_{as}) and v symmetric (v_s) of carbonyl (COO^-) stretches and the difference between them $\Delta v(COO^-)$. The frequency of these bands depends upon the coordination mode of carboxylate. Monodentate complexes exhibit $\Delta v(COO^-)$ values that are much greater than ionic complexes. Chelating (bidentate) complexes exhibit $\Delta v(COO^-)$ values that are significantly less than the ionic (phenyl acetate) values. $\Delta v(COO^-)$ values for bridging complexes are greater than those of chelating complexes, and close to the ionic values [26].

The stretching vibrations for sodium phenyl acetate $v_{as}(COO^-)$ and $v_s(COO^-)$ have been observed at 1562.2 cm^{-1} and 1387.1 cm^{-1}, respectively, with $\Delta v COO^-$ value of 175.1 cm^{-1}.
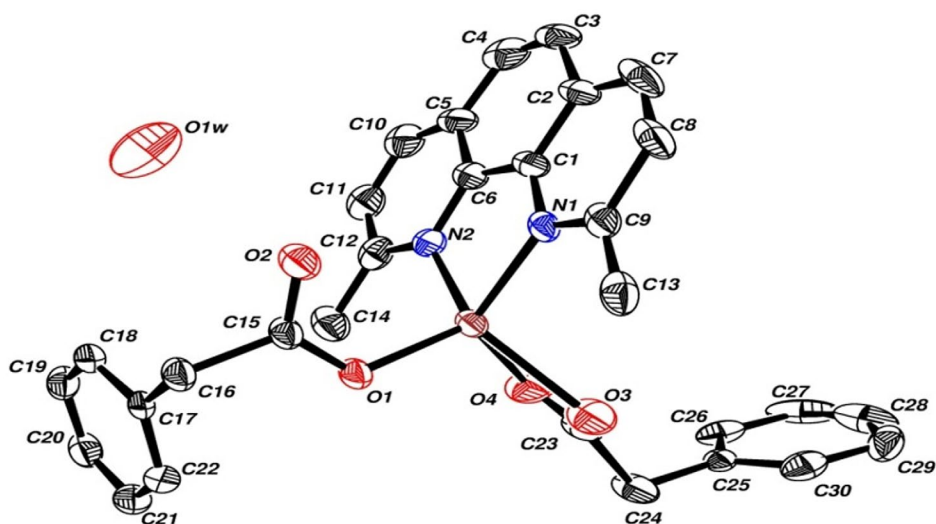
Figure 3. View of the molecular structure of **5** showing the atom numbering scheme. Ellipsoids represent thermal displacement parameters at the 25% probability level and hydrogens in calculated positions have been omitted for clarity.

Table 5. Summary of principle peaks in the IR spectra of **3–5** (cm^{-1}).

Assignments	Na-phenyl acetate	3	4	5
$v(C–H)_{ar}$	3025	3024	3057	3027
$\gamma(C–H)$	933,710	851	853	861
$v(C–H)_{alph}$	2000	2700	1998	2800
$v_{as}(N–H)$	–	3341	–	–
$v_s(N–H)$	–	3227	–	–
$\delta(NH_2)$	–	1619	–	–
(N–H) wagging	–	661, 698	–	–
$v(C–NH_2)$	–	1271	–	–
$v(C–C)_{ring}$	1496	1159	1223	1450
$v(C–C)_{ring} + \delta(CH)$	1281,1186	1499,1360	1144,1100	1340,1221
$v(C–N)$	–	1567	1515	1500
$v(Zn–O)$	–	459	421	400
$v(Zn–N)$	–	527	580	550

In **3**, $\Delta\upsilon COO^- = 199$ cm^{-1} > $\Delta\upsilon COO^-_{(Na\,phenyl)}$, so monodentate coordination is expected. In **4**, $\Delta\upsilon COO^- = 139.5$ cm^{-1} < $\Delta\upsilon COO^-_{(Na\,phenyl)}$ indicating bidentate coordination. However, according to X-ray, the coordination mode was bidentate for the first carboxylate group and monodentate for the second. Complex **5** with $\Delta\upsilon COO^- = 226$ cm^{-1} >> $\Delta\upsilon COO^-_{(Na\,phenyl)}$ indicates monodentate coordination. All previously mentioned coordination modes of **3**–**5** are in agreement with their X-ray structure determination.

Generally, the v(M–O) and v(M–N) for metal complexes are weak bands at 430–474 and 524–576 cm^{-1}, respectively [27]. These bands for **3**–**5** are shown in table 5.

3.4. ^{1}H and ^{13}C nuclear magnetic resonance

The relative intensities of ^{1}H NMR signals are in accord with the proposed structures, figures 4 and 5. Due to complex formation, change in the chemical shift takes place. As shown in table S4 slight upfield and downfield shifts were observed due to complexation with Zn or/ and nitrogen donor ligands.

3.5. Electronic absorption spectroscopy

Zn(II) complexes with completely filled d orbitals have no d–d electronic transitions. From the results tabulated in tables 6 and 7, no ligand to metal charge transfer "LMCT" can be observed due to filled d orbitals. The bands are assigned to MLCT charge transfer and intra-ligand transitions e.g. π–π* transition; the spectra of the complexes are similar to those of nitrogen parent ligands with very small shifts caused by zinc coordination. MLCT bands were observed at 201–296 nm with ϵ values around 3000 Lmol^{-1} cm^{-1} [28, 29].

3.6. BNPP hydrolysis

The abilities of **3**–**5** for phosphate diester hydrolysis were studied. The initial rate of hydrolysis was determined by measuring the absorption of 4-nitrophenolate at 400 nm and various plots of absorbance versus time were obtained

The Michaelis–Menten equation was used for calculating the initial rate against different concentrations of BNPP and the results are summarized in table 8. A suggested mechanism is shown in scheme 4: (1) H$_2$O coordinates with metal complex to produce complex **A**, (2) the oxygen on the P=O of the substrate (BNPP) is coordinated to the complex metal ion, forming intermediate **B**, (3) intramolecular metal hydroxide attacks the positive P of BNPP molecule to enhance release of the p-nitrophenol with first-order rate constant (k) for this step which is considered the key step for the hydrolysis, (4) after that H$_2$O coordinates again with the metal ion quickly, forming **D**, (5) the intermediate **D** quickly loses p-nitrophenol and phosphoric acid where H$_2$O is again bonded to the metal(II) rapidly, and thus completes the catalytic cycle [29, 30–32].

3.7. Antibacterial activity

The antibacterial activities of the synthesized zinc complexes were screened against different Gram-negative bacteria (*K. pneumonia*, *E. coli*, *P. mirabilis* and *P. aeruginosa*) and Gram-positive bacteria (*S. epidermidis*, *S. aureus*, *E. ferabis*, *M. luteus* and *B. subtilis*) to show the effect of complexation on antibacterial activity. The average IZD inhibition zone diameters of three
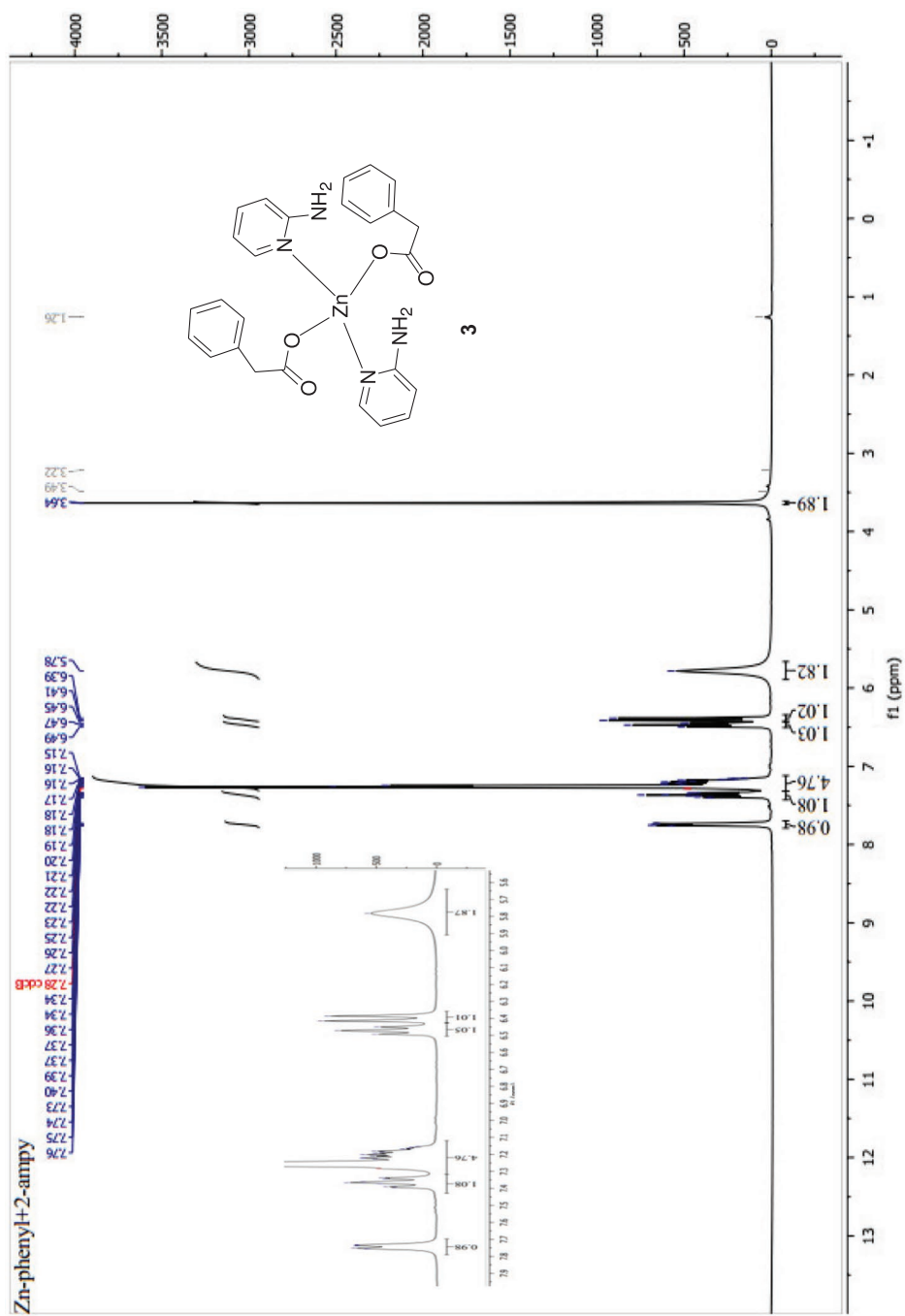
Figure 4. ¹H NMR spectrum of **3**.

Figure 5. ^{1}H NMR spectrum of **5**.

Table 6. UV–Visible spectral data for the prepared complexes.

Compounds	λ_{max} (nm)	ϵ (Lmol^{-1} cm^{-1})
Zn-phenyl	214	2280.3
	259	202.9
	265	203.68
3	296	7864.7
4	277	27,471
	292	19,379
	325	1594.4
5	201	23,816
	231	53,062
	269	31,408

Table 7. UV–Visible spectral data for N-ligands.

Ligands	λ_{max} (nm)	ϵ (Lmol^{-1} cm^{-1})
1,10-phen (1 × 10^{-5} M)	266.0	45,919
	225.0	45,488
2-ampy (1 × 10^{-4} M)	234.0	11,479
	291.0	5569.5
	200.0	5269.4
2,9-dmp (1 × 10^{-5} M)	272.0	184,090
	231.0	58,280

Table 8. Kinetic parameters of the BNPP hydrolysis by **3–5** at different [BNPP].

Concentration (M)	Initial rate, V_0 (mol L^{-1} s^{-1})	Max.rate, V_{max} (mol L^{-1} s^{-1})	Michaelis constant, Km (mol L^{-1})	Catalytic rate constant, Kcat[a] (s^{-1})	2-Order rate constant[b], K[BNPP] (L mol^{-1} s^{-1})
Complex **3** (1 × 10^{-3} M)					
1 × 10^{-3}	5.2 × 10^{-4}	5.1 × 10^{-4}	3.1 × 10^{-6}	0.513	1.7 × 10^5
1 × 10^{-4}	4.9 × 10^{-4}				
1 × 10^{-5}	3.8 × 10^{-4}				
Complex **4** (1 × 10^{-4} M)					
1 × 10^{-3}	3 × 10^{-4}	3 × 10^{-4}	9.6 × 10^{-6}	2.999	3.1 × 10^5
1 × 10^{-4}	2.7×10^{-4}				
1 × 10^{-5}	1.5×10^{-4}				
Complex **5** (1 × 10^{-3} M)					
1 × 10^{-3}	5.2×10^{-4}	5.3 × 10^{-4}	1.2 × 10^{-5}	0.526	4.3 × 10^4
1 × 10^{-4}	4.7×10^{-4}				
1 × 10^{-5}	2.4×10^{-4}				

[a]$K_{cat} = V_{max}/$[complex].
[b]$K_{BNPP} = K_{cat}/K_{m.}$

trials of the complexes were measured and stated as average ± standard error and summarized in table 9.

ZnCl$_2$ and Zn-phenyl did not show antibacterial activity against the tested microorganisms. DMSO was used as negative control to resist any tested microorganisms, whereas gentamicin (G) and erythromycin (E) were used as positive control for both G− and G+ bacteria. Complex **3** showed no activity against all tested bacterial species. Complex **4**
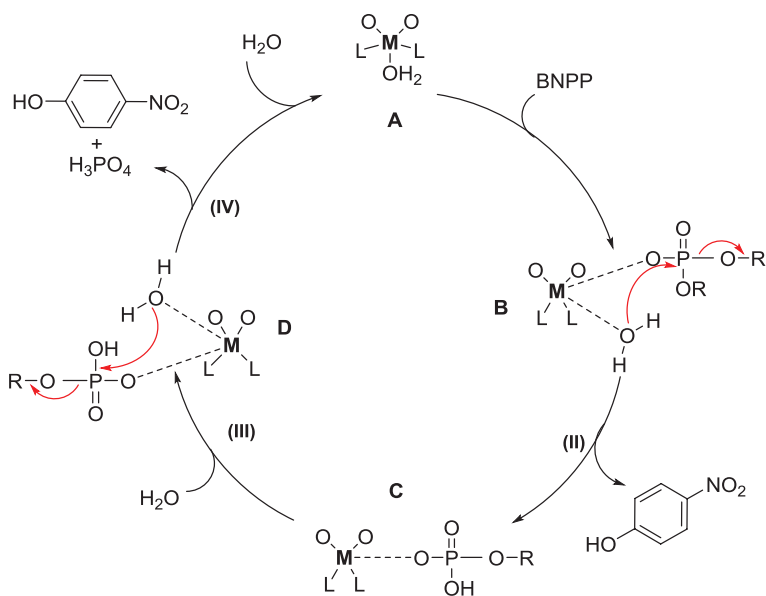
Scheme 4. The proposed mechanism of hydrolysis of BNPP.

Table 9. Antibacterial activity data of **3–5**.

	B. subtilis	S. epidermidis	S. aureus	E. faecalis	M. luteus
Compounds	G+	G+	G+	G+	G+
Zn-phenyl	–	–	–	–	–
Zn-methoxy	–	–	–	–	–
ZnCl$_2$	–	–	–	–	–
DMSO	–	–	–	–	–
G	29 ± 4	35 ± 1	29 ± 3	16.3 ± 0.9	35 ± 3
E	36 ± 2	45.0 ± 0.7	41 ± 1	–	40.0 ± 0.1
3	–	–	–	–	–
4	20.0 ± 0.9	29.6 ± 0.6	19.7 ± 0.5	–	25.3 ± 0.6
5	16 ± 2	31 ± 1	20.3 ± 0.5	–	14.6 ± 0.6
1,10-phen (pure)	33 ± 1	16.3 ± 0.8	16.8 ± 0.3	19.0 ± 0.8	35.7 ± 0.3
Compounds	K. pneumonia	P. mirabilis	E. coli	P. aeruginosa	
	G–	G–	G–	G–	
Zn-phenyl	–	–	–	–	
Zn-methoxy	–	–	–	–	
ZnCl$_2$	–	–	–	–	
DMSO	–	–	–	–	
G	35 ± 3	27 ± 1	25.3 ± 0.9	20 ± 2	
E	21.5 ± 0.5	17.3 ± 0.9	24 ± 2	22 ± 3	
3	–	–	–	–	
4	21 ± 1	24.6 ± 0.6	24 ± 1	–	
5	–	–	–	–	
1,10-phen (pure)	32 ± 1	33.0 ± 0.6	31.0 ± 0.6	–	

showed good activity against G– bacteria except *P. aeruginosa*, and against G+ bacteria except *E. ferabis*. Complex **5** showed no activity against G– bacteria, low activity against *M. luteus* and *B. subtilis* bacteria and high activity against *S. epidemidis* and *S. aureus*.

4. Conclusion

New Zn(II) complexes with phenyl acetic acid in the presence of 2-ampy, 2,9-dmp and 1,10-phen have been synthesized and characterized. IR, UV–Vis, ^{1}H and ^{13}C{^{1}H}-NMR spectroscopic techniques were used to study the new complexes. X-ray single crystal diffraction measurements were also determined for **3**–**5** as evidence for their structures. Different metal geometries and carboxylate coordination modes have been proved. The structure of **3** is a slightly distorted tetrahedral geometry with two monodentate phenyl acetate groups and two monodentate 2-ampy ligands. Complexes **4** and **5** showed similar distorted trigonal bipyramidal geometries with one monodentate and one bidentate phenyl acetate group, and one bidentate 1,10-phen or 2,9-dmp, respectively. The obtained results from the kinetic experiments showed that these complexes can be potent BNPP hydrolysis agents with the activitiy decreasing in the order **4** > **3** > **5**.

Complex **3** did not show any activity against G− or G+ bacteria. Complex **4** showed good activity against G− bacteria except *P. aeruginosa* and G+ bacteria except *E. faecalis*. Complex **5** showed no activity against G− bacteria, low activity against *M. luteus* and *B. subtilis* and high activity against *S. epidermidis* and *S. aureus*.

Supplementary material

CCDC 1488198, CCDC 1488200 and CCDC 1488196 contain the supplementary crystallographic data for **3**, **4** and **5**, respectively. These data can be obtained free of charge via http://www.ccdc.cam.ac.uk/conts/retrieving.html, or from the Cambridge Crystallographic Data Center, 12 Union Road, Cambridge CB2 1EZ, UK; Fax: (+44)1223–336-033; or E-mail: deposit@ccdc.cam.ac.uk. Supplementary data associated with this article can be found in the online version.

Disclosure statement

No potential conflict of interest was reported by the authors.

ORCID

Hijazi Abu Ali 🆔 http://orcid.org/0000-0002-6315-6868

References

[1] S. Astrid, S. Helmut. *Metal Ions in Biological Systems*, Vol 32, Marcel Dekker Inc., New York, NY (1996).
[2] M. Frezza, S. Hindo, D. Chen, A. Davenport, S. Schmitt, D. Tomco, Q. Ping Dou. *Curr. Pharm. Des.*, **16**, 1813 (2010).
[3] R.M. Roat-Malone, Bioinorganic Chemistry: A Short Course, R.M. Roat-Malone (Ed.), 1st Edn., John Wiley and Sons, New Jersey (2002), pp 1–23.
[4] C.T. Walsh, H.H. Sandstead, A.S. Prasad, P.M. Newberne, P.J. Fraker. *Environ. Health Perspect.*, **102**(Suppl 2), 5 (1994).
[5] S.B. Etcheverry, D.A. Barrio, A.M. Cortizo, P.M.A. Williams. *J. Inorg. Biochem.*, **88**, 94 (2002).
[6] V. Uivarosi. *Molecules*, **18**, 11153 (2013).
[7] M. Rizzotto, In *A Search for Antibacterial Agents*, V. Bobbarala (Ed.); INTECH Open Access Publisher (2012).
[8] F. Dimiza, A.N. Papadopoulos, V. Tangoulis, V. Psycharis, C.P. Raptopoulou, D.P. Kessissoglou, G. Psomas. *Dalton Trans.*, **39**, 4517 (2010).

[9] F. Dimiza, A.N. Papadopoulos, V. Tangoulis, V. Psycharis, C.P. Raptopoulou, D.P. Kessissoglou, G. Psomas. *J. Inorg. Biochem.*, **107**, 54 (2012).

[10] S. Tsiliou, L.A. Kefala, F. Perdih, I. Turel, D.P. Kessissoglou, G. Psomas. *Eur. J. Med. Chem.*, **48**, 132 (2012).

[11] M. Zampakou, N. Rizeq, V. Tangoulis, A.N. Papadopoulos, F. Perdih, I. Turel, G. Psomas. *Inorg. Chem.*, **53**, 2040 (2014).

[12] F. Dimiza, S. Fountoulaki, A.N. Papadopoulos, C.A. Kontogiorgis, V. Tangoulis, C.P. Raptopoulou, V. Psycharis, A. Terzis, D.P. Kessissoglou, G. Psomas. *Dalton Trans.*, **40**, 8555 (2011).

[13] S. Fountoulaki, F. Perdih, I. Turel, D.P. Kessissoglou, G. Psomas. *J. Inorg. Biochem.*, **105**, 1645 (2011).

[14] C. Tolia, A.N. Papadopoulos, C.P. Raptopoulou, V. Psycharis, C. Garino, L. Salassa, G. Psomas. *J. Inorg. Biochem.*, **123**, 53 (2013).

[15] M. Darawsheh, H. Abu Ali, A.L. Abuhijleh, E. Rappocciolo, M. Akkawi, S. Jaber, S. Maloul, Y. Hussein. *Eur. J. Med. Chem.*, **82**, 152 (2014).

[16] H. Abu Ali, M.D. Darawsheh, E. Rappocciolo. *Polyhedron*, **61**, 235 (2013).

[17] H. Abu Ali, H. Fares, M.D. Darawsheh, E. Rappocciolo, M. Akkawi, S. Jaber. *Eur. J. Med. Chem.*, **89**, 67 (2015).

[18] H. Abu Ali, B. Jabali. *Polyhedron*, **107**, 97 (2016).

[19] H. Abu Ali, S.N. Omar, M.D. Darawsheh, H. Fares. *J. Coord. Chem.*, **69**, 1110 (2016).

[20] B. Jabali, H. Abu Ali. *Polyhedron*, **117**, 249 (2016).

[21] J. Florián, A. Warshel. *J. Phys. Chem. B*, **102**, 719 (1998).

[22] J. Li, H. Li, B. Zhou, W. Zeng, S. Qin, S. Li, J. Xie. *Transition Met. Chem.*, **30**, 278 (2005).

[23] SMART-NT V5.6, Bruker AXS GMBH, D-76181 Karlsruhe, Germany (2002).

[24] SHELXTL-NT V6.1, BRUKER AXS GMBH, D-76181 Karlsruhe, Germany (2002).

[25] S. Li, W. Hu, W. Ying. *Prog. React. Kinet. Mech.*, **41**, 120 (2016).

[26] H. Kagi, D. Ushijima, R. Iizuka, S. Nakano, T. Nagai. *High Press. Res.*, **28**, 299 (2008).

[27] J.B. Hodgson, G.C. Percy. *Spectrochim. Acta, Part A*, **34**, 777 (1978).

[28] S.L. Reddy, T. Endo, G.S. Reddy. Electronic (Absorption) Spectra of 3d Transition Metal Complexes, Advanced Aspects of Spectroscopy, Dr. Muhammad Akhyar Farrukh (Ed.) (2012).

[29] A.B.P. Lever. *J. Chem. Educ.*, **51**, 612 (1974).

[30] J. Li, J. Xie, W. Zeng, X. Wei, B. Zhou, X. Zeng, S. Qin. *Transition Met. Chem.*, **29**, 488 (2004).

[31] D. Kou, X.-G. Meng, Y. Liu, J. Du, X.-M. Kou, X.-C. Zeng. *Colloids Surf., A*, **324**, 189 (2008).

[32] W. Jiang, B. Xu, J. Zhong, J. Li, F. Liu. *J. Chem. Sci.*, **120**, 411 (2008).